Supporting Information

Simultaneous Assembly of van der Waals Heterostructures into Multiple Nanodevices

Enrique Burzurí, Mariano Vera-Hidalgo, Emerson Giovanelli, Julia Villalva, Andres Castellanos-Gomez* and Emilio M. Pérez**

This Supporting Information is divided in the following sections: (1) Experimental procedures, (2) fabrication details and schematics of the multi-electrode devices, (3) dielectrophoresis mechanism and possible solvents, (4) finite elements analysis of the electrical field distribution, (5) additional SEM images of the devices, (6) additional AFM characterization of the device, (7) electric characterization of additional devices, (8) a comparative with dropcasted devices and (9) Supplementary table with the interpretation of the Raman spectra.

(1) Experimental procedures

Preparation of franckeite colloidal suspension. Chips from natural franckeite mineral (San José mine, Oruro, Bolivia) were ground in an agate mortar until a fine black powder was obtained. Franckeite powder (10 mg) was dispersed in *i*PrOH (10 mL) in a 20-mL glass vial. The dispersion was subjected to ultrasound irradiation for 1 h in an ultrasonic bath (Fisher Scientific FB 15051; 37 kHz, 280 W, ultrasonic peak max. 320 W, standard sine-wave modulation) connected to a cooling system maintaining the water bath temperature at 20 °C. The resulting black suspension was centrifuged at 990 *g* and 20 °C for 30 min (Beckman Coulter Allegra X-15R, FX6100 rotor, radius 9.8 cm); it separated into a black sediment and an orange supernatant, which was carefully isolated from the solid. The corresponding franckeite suspension remained colloidally stable for 48 h to 72 h, after which it progressively deposited. Nonetheless, the franckeite flakes could easily be redispersed by 1-2 min bath sonication.

Transmission Electron Microscopy (TEM). The colloidal suspension was drop-casted onto a 200 square mesh copper grid covered with a carbon film. After a few minutes, the

excess solvent was removed and the grid was left drying in the air at room temperature. The procedure was repeated 5 times and the grid was finally dried under vacuum for 48 h. The observation was performed using a JEOL JEM 2100 microscope operated at 200 kV.

UV-Vis-NIR spectroscopy. As-prepared colloidal suspension was transferred to a quartz cuvette and its extinction spectrum (sum of the absorption and scattering spectra) was measured using a Cary 5000 spectrophotometer from Agilent Technologies.

Raman spectroscopy. Bulk franckeite powder (pressed onto a glass slide), liquid-phase-exfoliated franckeite (drop-cast on a glass slide and dried at 40 °C several times) and on-device franckeite (after DEP) were characterized using a Bruker Senterra confocal Raman microscope (Bruker Optik, Ettlingen, Germany; objective NA 0.75, 50×; laser excitation: 532 nm, 0.2 mW). The spectra result from the average of 10 measurements acquired from different regions over the whole samples.

Device fabrication. The multi-electrode devices are fabricated *via* laser mask-less optical lithography and thermal evaporation of Cr/Au (5/70 nm). A lift-off process in acetone/*i*PrOH/deionized water removes the excess metallic material. The devices are fabricated on a highly-doped silicon substrate capped with a 300 nm thick insulating SiO_2 layer. This substrate is used as common back-gate electrode. Additional details and the final device are shown in the Supporting Information.

Atomic Force Microscopy. The AFM images were acquired in intermittent (tapping) mode and under ambient conditions by using a NT-MDT NTEGRA PRIMA station equipped with a SF005$AU007NTF head and NT-MDT NSG01 silicon cantilevers with typical spring constant and resonant frequency of 5.2 Nm^{-1} and 144 kHz respectively.

Electron Transport Measurements. The current-voltage curves and transfer characteristics were obtained in ambient conditions in the chamber of an electrical probe station equipped with a Keithley 2450 digital source-meter unit.

(2) Fabrication details and schematics of the multi-electrode devices

The multi-electrode devices (see Figure S1) are fabricated *via* laser mask-less optical lithography and thermal evaporation of Cr/Au (5/70 nm) electrodes. The finger-shaped electrodes are connected to common Au pads that allow performing simultaneous dielectrophoresis to all the devices. A lift-off process in acetone/iPrOH/deionized water removes the photoresist and the excess metallic material. The devices are fabricated on a highly-doped silicon substrate coated with a thin insulating SiO_2 layer. This substrate is used as common back-gate electrode. A scheme and a scanning electron microscopy (SEM) image of final device are shown in Figure S1.

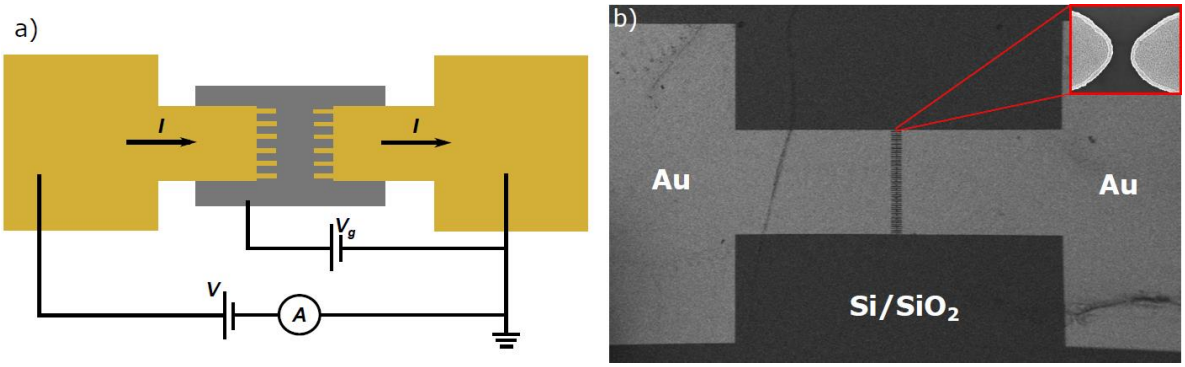

Figure S1. (a) Schematics and (b) scanning electron microscopy (SEM) image of the full multi-electrode device.

(3) Dielectrophoresis mechanism and possible solvents

The dielectrophoretic (DEP) force F_{DEP} exerted on oblate ellipsoidal particles with a large aspect ratio (which best approximates exfoliated layers) can be written as follows:

$$F_{DEP} \propto V_p \, \varepsilon_m \, Re\left[\frac{\varepsilon_p^* - \varepsilon_m^*}{\varepsilon_m^*}\right] \nabla |\boldsymbol{E}|^2$$

where V_p is the volume of the particles; ε_p^* and ε_m^* are respectively the complex permittivities of the particles and the suspension medium; and $\boldsymbol{E}$ is the non-uniform electric field. The DEP force is thus proportional to the nanoflake volume, aligned with the electric field gradient and its orientation depends on the sign of the real part of the Clausius-

Mossotti factor $\left[\left(\varepsilon_p^* - \varepsilon_m^*\right)/\varepsilon_m^*\right]$. The Clausius-Mossotti factor is in turn related with the polarizability of the particles and solvent.

The selection of *i*PrOH as solvent is made on the basis of its weaker polarizability (6.98 $Å^3$[1]) compared to the constituents of franckeite (~10 $Å^3$) [2,3], necessary for dielectrophoresis, and a boiling point (82 ºC) that makes *i*PrOH non-volatile enough to perform DEP but easy enough to evaporate. In addition, LPE in *i*PrOH produces colloidal flakes having few-unit-cell thicknesses as we explain in the main text.

These are general conditions that any solvent need to meet in order to be suitable for LPE+DEP. Liquid phase exfoliation of franckeite has been achieved in *i*PrOH, different water/ *i*PrOH mixtures and methanol as reported in [4], as well as in acetonitrile (data not reported). This could probably be expanded to alcohols in general although it remains to be proved.

Once the LPE is achieved, DEP of the colloids could be performed with solvents presenting a polarizability lower than 10 $Å^3$ and a boiling point between 60 ºC and 90 ºC. Some solvents meeting those requirements (see [1]) are 2,2,2-trifluoroethanol (5.20 $Å^3$; 78°C), 2-propenenitrile (6.24 $Å^3$; 77°C), acetonitrile (4.44 $Å^3$; 82°C), ethanol (5.13 $Å^3$; 78°C) and methanol (3.26 $Å^3$; 65°C). Other solvents like acetone (6.47 $Å^3$; 56°C), ethyl formate (7.09 $Å^3$; 54°C) and methyl acetate (7.00 $Å^3$; 57°C) could be used although the lower boiling point could present problems due to a fast evaporation.

Some of these solvents are not necessarily good for LPE and a single solvent for the whole process would be desirable. Taking this into account, acetonitrile, *i*PrOH, methanol and ethanol are good candidates for combined LPE and DEP that in addition are commonly used solvents.

(4) Finite elements analysis of the electrical field distribution in the device

The electrical field distribution in the device surface is calculated by using a finite elements analysis software. A real-scale pattern (2D in-plane for simplicity) of the device is imported in the software where the electrostatic parameters (voltage potential, charge conservation, dielectric constants) of the boundaries are assigned. The pattern is thereafter divided in a software-optimized polygonal mesh. The computed electrical field is plotted in Figure 2 of the main manuscript.

Figure S2(a,c) shows the E^2 and $\nabla|E|^2$ profiles taken along the *y* axis and crossing the gap area between the electrodes (yellow line in the inset of Figure S2d). The electrical field is maximum within the gap between the electrodes. The gradient is directed towards the gap where it becomes zero. The flakes are therefore trapped once they reach the inter-electrode space. This allows the controlled accumulation of material by graduating the time of dielectrophoresis and concentration of flakes in the liquid phase exfoliation

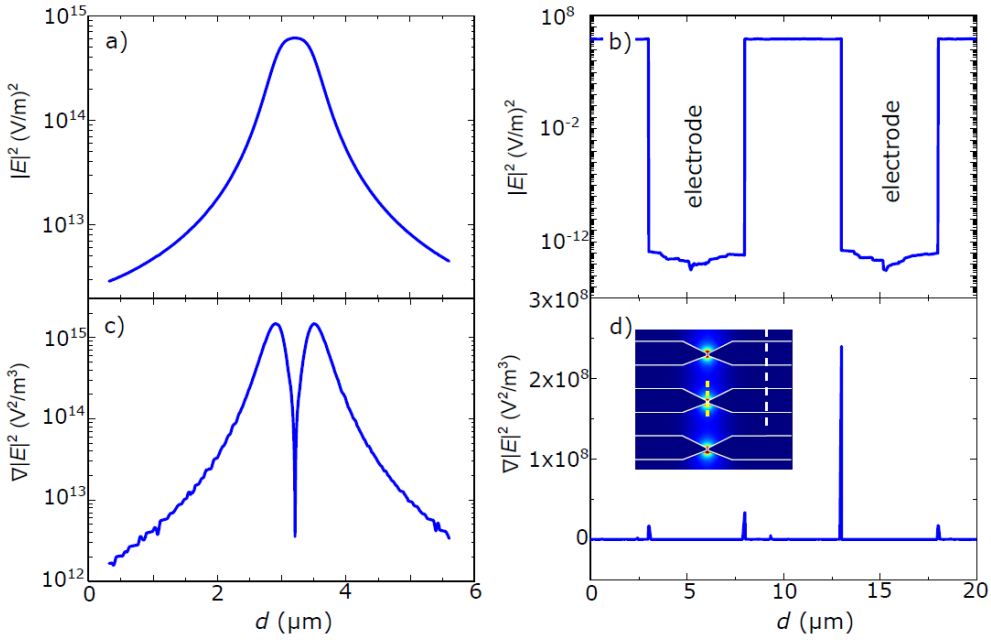

Figure S2. (a) Squared electrical field (E^2) and (c) $\nabla|E|^2$ across the gap in the *y*-axis along the yellow line in (d) inset. (b) Squared electrical field (E^2) and (d) $\nabla|E|^2$ in the *y*-axis in the "inter-finger" area marked by the white line in the inset. The inset shows the E^2 distribution in the device. The electrodes' edges are highlighted in solid white as a guideline to the eye.

Figure S2(b,d) shows the E^2 and $\nabla|E|^2$ profiles taken in the area far from the gap and in between the Au "finger-like" electrodes (white line in the inset of Figure S2d). The in-plane electrical field is around four orders of magnitude smaller than in the area around the gap. This makes $|E|^2$ eight orders of magnitude smaller. However, the sharp transition between the dielectric and the electrode area creates a strong electrical gradient at the edge of the electrodes. The flakes are therefore directed towards the edge of the electrode as has been observed experimentally.

(5) Additional SEM images of the franckeite-based devices

Figure S3 shows additional SEM images of pairs of electrodes after dielectrophoresis. The franckeite flakes are mainly packed in the inter-electrode space, where the dielectrophoretic force is directed, and along the electrode edges as shown in the main text and discussed before. The surrounding substrate is clean of material.

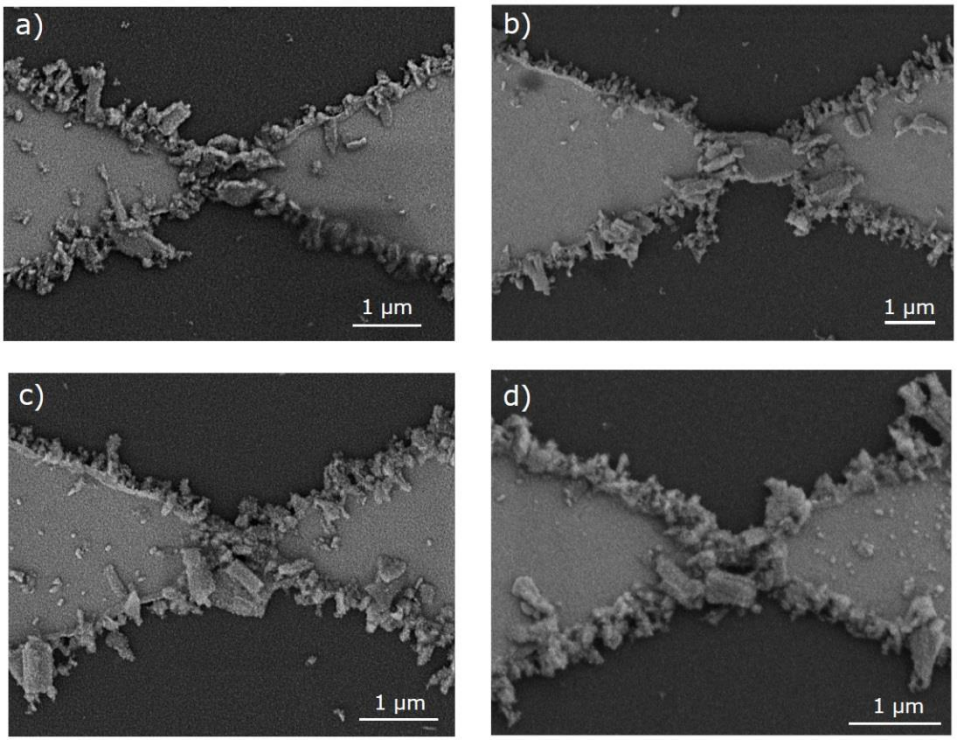

Figure S3. Scanning electron microscopy (SEM) images taken in different electrode-pairs of different devices. The material is mainly found in the inter-electrode space and the electrode edges.

(6) Additional AFM images of the franckeite-based devices

Figure S4 shows atomic force microscopy (AFM) images of the bare electrodes before DEP and the liquid-phase exfoliated franckeite flakes drop-casted on a Au substrate. The height profile of the flakes fluctuates between 50 nm and 150 nm, possibly due to the stacking of several flakes.

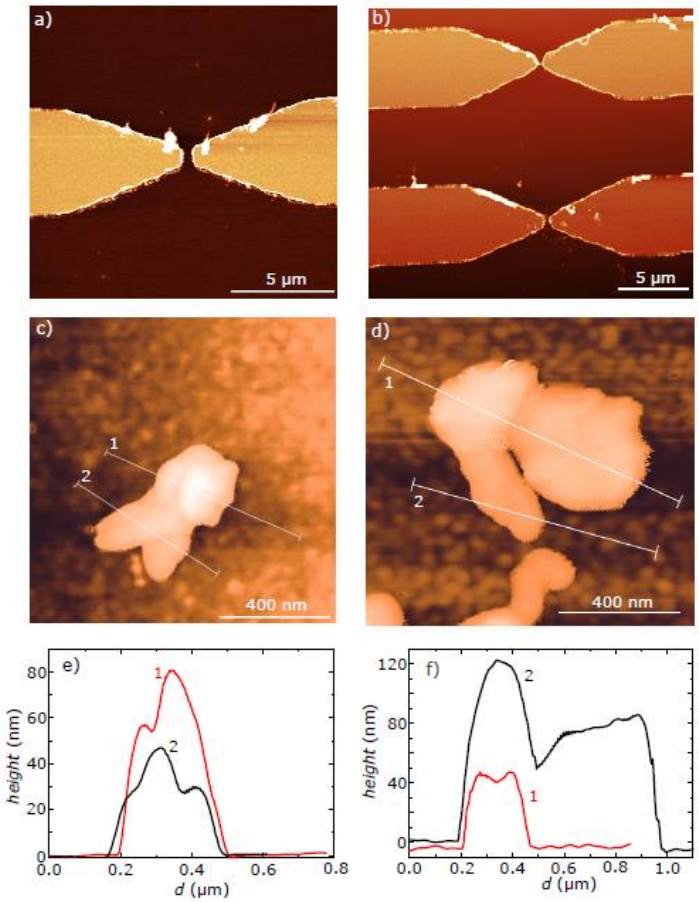

Figure S4. (a), (b) Atomic force microscopy (AFM) images of the empty electrodes. (c), (d) AFM images and (e), (f) height profiles of franckeite flakes deposited on a Au substrate.

After dielectrophoresis, the flakes gather mainly in the gaps creating stacks that reach around 1 μm wide and around 400 nm high as seen in different devices in Figure S5. These values compared with the average dimensions of flakes indicate that three to five flakes may be stacked in height within the gap.

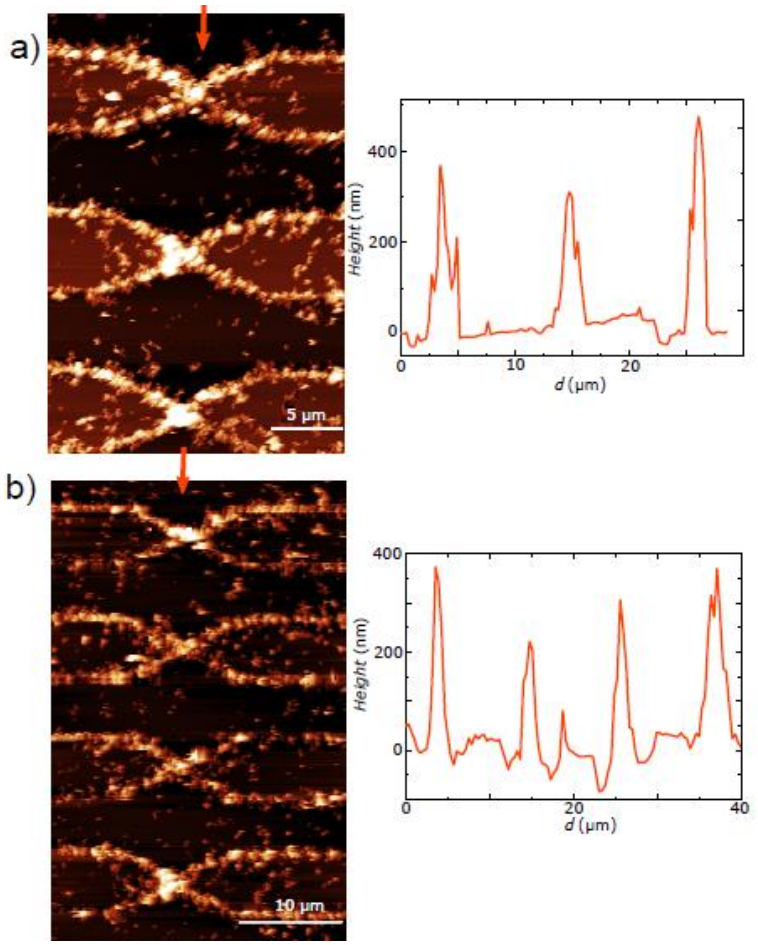

Figure S5. Atomic force microscopy (AFM) images and corresponding height profiles across the gaps taken in different devices.

(7) Electrical characterization of additional devices

Figure S6 shows the current (*I*) - voltage (*V*) curves and the corresponding transfer characteristic measured in an additional franckeite-based multi-electrode device. The

negative slope of the transfer characteristics is indicative of a p-doped semiconducting behavior as reported for bulk franckeite. Besides, the non-linear *I-V* curves are indicative of the formation of Schottky barriers between the semiconducting franckeite and the metallic Au electrodes.

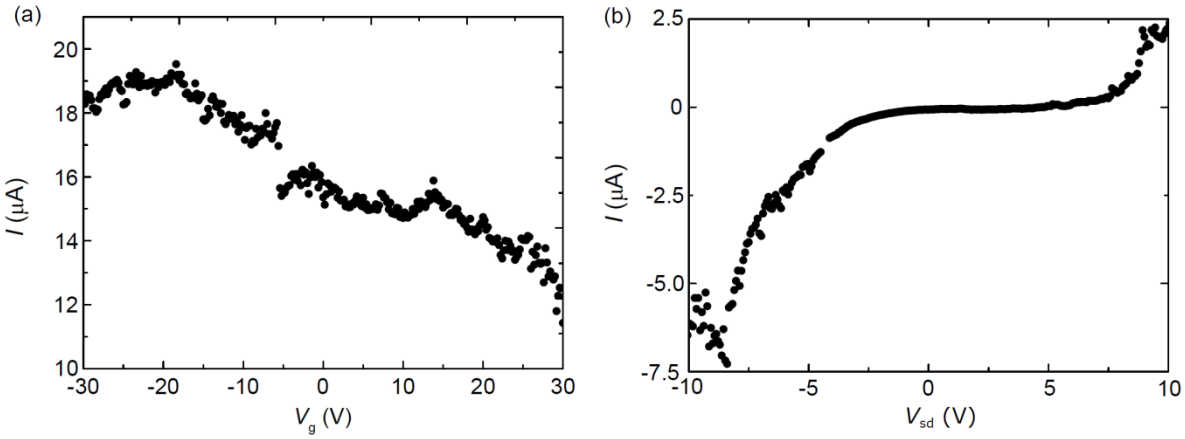

Figure S6. a) Transfer characteristic and b) current-voltage characteristic of an additional multi-electrode franckeite-based device. The transfer characteristic points to a p-doped semiconductor. The asymmetric *I-V* curve indicates the formation of Schottky barriers between the metallic electrodes and the semiconducting franckeite.

(8) Devices prepared by drop-casting

Figure S7a shows an optical microscope image of a device prepared by DEP. The franckeite is clearly concentrated around the electrodes tips. The DEP conditions are set assemble more material and therefore facilitate visualization under the optical microscope. In contrast, Figure S7b shows a multi-electrode device prepared by drop-casting of a liquid-phase exfoliated franckeite droplet in the absence of a dielectrophoretic field. The franckeite appears evenly distributed over all the surface and no significant accumulation between the electrodes is observed.

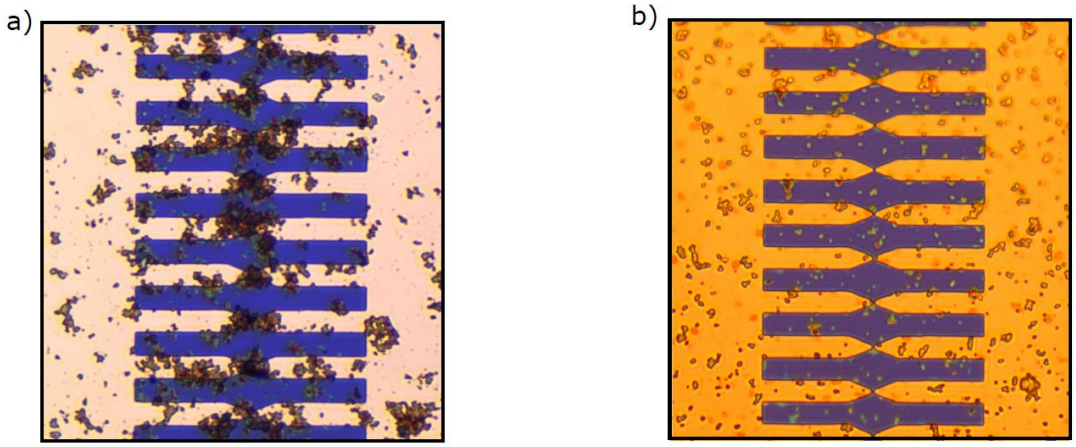

Figure S7. Optical microscope images of multi-electrode devices made by (a) dielectrophoresis and (b) drop-casting in the absence of a dielectrophoretic field. The franckeite is clearly concentrated around the electrodes tips in a) whereas is evenly dispersed in b). The DEP conditions in a) are set to assemble more material than in the main manuscript to facilitate the visualization under the optical microscope.

(9) Supplementary tables

Supplementary Table 1 shows the labelling and interpretation of the different Raman modes of franckeite as reported in the Supporting Information of Ref [4].

Supplementary Table 1. Interpretation of the Raman spectra of franckeite [4]

Raman shift (cm^{-1})	Phonon mode attribution	Compound
70	Acoustic	PbS
143	2^{nd} order effect	SnS_2
	Transverse acoustic and transverse optical	PbS
195	Longitudinal optical	PbS
	E_g	SnS_2
256	Combination	PbS+SnS_2
318	A_{1g}	SnS_2

References

[1] R. Bosque and J. Sales, *J. Chem. Inf. Comput. Sci.*, 2002, **42**, 1154-1163

[2] R. R. Reddy, K. Rama Gopal, K. Narasimhulu, L. Siva Sankara Reddy, K. Raghavendra Kumar, G. Balakrishnaiah and M. Ravi Kumar, *J. Alloys Compd.*, 2009, **473**, 28-35.

[3] V. P. Gupta, P. Agarwal, A. Gupta and V. K. Srivastava, *J. Phys. Chem. Solids*, 1982, **43**, 291-295.

[4] A. J. Molina-Mendoza, E. Giovanelli, W. S. Paz, M. A. Niño, J. O. Island, C. Evangeli, L. Aballe, M. Foerster, H. S. J. van der Zant, G. Rubio-Bollinger, N. Agraït, J. J. Palacios, E. M. Pérez and A. Castellanos-Gomez, *Nat. Commun.*, 2017, **8**, 14409.